Open Ceramics 9 (2022) 100226

Contents lists available at ScienceDirect

Open Ceramics

journal homepage: www.sciencedirect.com/journal/open-ceramics

Pilot scale fabrication of lanthanum tungstate supports for H_2 separation membranes

J. Gurauskis [*,1], Vanesa Gil [**,2], Bin Lin, Mari-Ann Einarsrud

Department of Materials Science and Engineering, Norwegian University of Science and Technology, Sem Saelands vei 12, Trondheim NO-7030, Norway

ARTICLE INFO

Keywords:
Asymmetric tubular membrane
Lanthanum tungstate
Thermoplastic extrusion
Hydrogen separation
Hydrogen transport membrane

ABSTRACT

This paper reports the fabrication of asymmetric tubular geometry lanthanum tungstate-based membranes for high temperature H_2 separation applications. As starting materials, powders with the compositions $La_{28-y}W_{4+y}O_{54+\delta}$ ($y = 0.848$), $La_{28-y}W_{4+y}O_{54+\delta}$ ($y = 1$) and $La_{28-y}(W_{1-x}Mo_x)_{4+y}O_{54+\delta}$ ($x = 0.3$, $y = 1$) were synthesized by solid state reaction method. Porous, thick-wall tubes made of lanthanum tungstate-based powders with high gas permeability (7–8 $x10^{-15}$ m^2 at 2 bar overpressure) and homogeneous porous microstructure were made by combining a cost-effective solid-state synthesis and thermoplastic extrusion method. Deposition of lanthanum tungstate-based dense thin film (~20 μm) was achieved on top of porous supports through dip coating technique. The influence of conformation routes, thermal debindering and sintering processes were investigated in detail to achieve defect free H_2 transport membranes. Asymmetric geometry membranes with ~20 μm dense layer thickness supported on porous tubular (~ 7.5 mm diameter and ~0.8 mm thick) supports.

As a result, a procedure for proton conducting ceramics manufacture was established which can be deployed to fabricate high temperature catalytic membrane reactors for synthetic fuel from gas-to-liquid (GTL) processes.

1. Introduction

The development of new hydrogen permeation devices to produce intermediate olefins/aromatics are of potential interest to the petrochemical industry as there is the worldwide need to find suitable alternatives that meet price and sustainability requirements. The use of ceramic membrane reactors to selectively separate hydrogen from hydrocarbon fuels without the need of any external electric circuits removes the thermodynamic barriers which otherwise limits the overall yield [1–5]. A potential ceramic membrane material requires appreciable mixed proton-electron conductivity, thermal and hydrothermal stability, as well as chemical stability in reducing and water-containing atmospheres at elevated temperatures.

Perovskite-type oxides, in particular acceptor-doped $Ba(Ce,Zr)O_3$ and $Sr(Ce,Zr)O_3$ have been extensively investigated because of their excellent proton-electron conductivity at high temperatures [6,7]. Unfortunately, these perovskite membranes are chemically unstable, easily reacting with CO_2 and H_2O or exhibit high grain boundary impedances limiting the dc conductivity [8]. Outside the family of perovskites, materials that exhibit proton conductivities with CO_2 stability, such as rare-earth ortho-niobates and ortho-tantalates, exhibit too low proton conductivity within the range of 10^{-4}-10^{-3} S/cm, which would limit their prospects as hydrogen separation membranes [9,10].

Rare-earth tungstates have been reported to show relatively high mixed proton and electron conductivity [11] and also proven chemically stable towards acidic gases, e.g., CO_2 [12,13]. To further enhance the electronic conductivity of lanthanum tungstates (LWO), molybdenum partly substitution for tungsten is a promising material [14].

The performance and costs of these membranes are strongly dependent not only on the material properties but also on the membrane architecture and the processing technologies to shape them. In this regard, there is a significant lack of application-oriented research on dense ceramic membranes for H_2 separation in general, and specifically on lanthanum tungstate-based membranes. Most of the investigations have been focused on bulk ceramic samples, however, to achieve high hydrogen fluxes membrane structures with a thickness ≤30 μm is desired. One of the most critical issues when membrane thickness is reduced is the loss of the mechanical stability. An asymmetric

* Corresponding author.
** Corresponding author.
E-mail addresses: jonas.gurauskis@csic.es (J. Gurauskis), vgil@hidrogenoaragon.org (V. Gil).
[1] Present address: ARAID at *INMA, Instituto de Nanociencia y Materiales de Aragón (CSIC-Unizar)* (Spain).
[2] Present address: ARAID at Aragon Hydrogen Foundation (Spain).

https://doi.org/10.1016/j.oceram.2022.100226
Received 30 October 2021; Received in revised form 22 December 2021; Accepted 26 December 2021
Available online 29 January 2022

membrane design consisting of a dense membrane layer and a porous support must be developed, so that the final architecture provides sufficient mechanical stability and durability for μm-thick membranes as well as sufficient porosity to ensure optimal gas supply.

At present, only a very few works elucidate the H_2 permeation in thin supported membranes based on dense layers below 50 μm supported on porous supports [15–21]. These works investigate planar asymmetric membranes however, the tubular geometry of the reactor for synthetic fuel from gas-to-liquid (GTL) offers more favorable conditions than planar design: larger surface area to volume ratio, good thermal cycling stability and the possibility for use cold seals [7]. Several works have been reported for the production of tubular asymmetric membranes with various manufacturing strategies such as tape casting rolled and coating, phase inversion casting, spin-spraying and cosintering and extrusion and dip coating [7,22–28]. From those, only a few reports deal with the production of tubular asymmetric membranes based on the promising lanthanum tungstate materials. However, there are no reports dealing with the production lanthanum tungstate based membranes utilizing tubular porous supports of similar (or close) composition as the thin membrane material. Because of the difficulty of developing full dense layers below 30 μm withouth large defects onto tubular porous substrates with sufficient mechanical strenght in addition to low permeation resistance.

Therefore, the lack of knowledge to manufacture reproducible and defect free functional thin membranes based on full lanthanum tungstate compositions, in special with tubular shape, by cheap and reproducible and industrially scalable processing routes is crucial to achieve a technological breakthrough in this area and the realistic application of H_2 separation membranes technologies.

The present paper aims to fill out the gap of fabrication strategies of lanthanum tungstate-based membranes with tubular geometry for hydrogen separation applications by developing a low-cost thermoplastic binder system for extrusion-based conformation and strategies for pilot scale demonstrators.

Extrusion seems to be an economically advantageous method of manufacturing tubular membranes with elongated profile geometry. The traditional solvent-based binder systems for extrusion of ceramic materials contain polymers which solvate or swell in a solvent (e.g., water or alcohol-based systems). In case of thermoplastic [29,30] the conformation process is based on the use of polymers (e.g., PE, PP or EVA) which, when heated, soften, melt or become more pliable, and harden during cooling in a reversible physical process. The main advantages of thermoplastic binder systems over solvent-based ones are: (a) the lower abrasivity of the feedstock material and (b) the contour accuracy of the extruded material [31,32]. Moreover, the reusability of the extrusion paste is favored in case of thermoplastic binder systems which is of interest due to relatively high price of lanthanum tungstate based feedstock materials.

Deposition of dense thin film lanthanum tungstate membrane was performed through dip coating process, a highly economical method due to its simplicity. For this, an optimization of organic solvent system was performed to achieve stable colloidal suspension. Full details of colloidal suspension optimization and deposition procedure are given elsewhere [17].

2. Experimental

2.1. Synthesis of LWO and LWOMo based powders

$La_{28-y}W_{4+y}O_{54+\delta}$ (y = 0.848, LWO56), $La_{28-y}W_{4+y}O_{54+\delta}$ (y = 1, LWO54) and $La_{28-y}(W_{1-x}Mo_x)_{4+y}O_{54+\delta}$ (x = 0.3, y = 1, LWOMo) powders were synthesized by solid state reaction using oxide precursors. The synthesis steps, similar for all the compositions, are as follows:

(1) Ball mill in ethanol media for 24 h nominal amounts of the two starting compounds, La_2O_3 (Sigma-Aldrich, 99.9%) and WO_3 (Sigma-Aldrich, 99.9%) or MoO_3 when needed (Sigma-Aldrich, 99.5%). Pre-annealing step of the La_2O_3 powder at 600 °C for 2 h is required.
(2) Dry the resulting powder mix at ~80 °C for 24 h and manually break down big agglomerates in Agatha mortar.
(3) The calcination process consists of two steps and a low starting temperature is crucial as WO_3 is quite volatile: (a) at 700 °C for 15 h in air and (b) at 1100 °C for 15 h in air. After each calcination step, a ball milling in ethanol for 24 h is conducted.

After the two calcination steps only a trace amounts of La_2O_3 are present, which is not necessarily an issue, as the La_2O_3 is likely to react further during sintering process. Also, there are indications that La_2O_3 will perform as a deterrent to full densification, which might be beneficial for producing the required highly permeable porous structures.

2.2. Thermoplastic extrusion of LWO and LWOMo porous tubular supports

The thermoplastic compounds used for the extrusion of the porous supports were prepared by mixing the as-synthesized powders (LWO56, LWO54 or LWOMo) with 20 vol% carbon black as a sacrificial pore former (Merck KGaA, Germany) and molten resin which consisted of 24 vol% copolymer ethylene-vinylacetate (EVA) (Elvax 250, Du Pont de Nemours, Wilmington, DE), 17 vol% paraffin wax (54/56, Slovnaft, Bratislava, Slovakia), and 9 vol% stearic acid (1.0067, Merck, Darmstadt, Germany).

Approximately 50 vol% of the powders was gradually added to the molten resin and mixed using a heated piston extruder (Loomis 232-16 DTM extruder, Germany) with spaghetti die at 140 °C (20 times). Following their preparation, the thermoplastic compounds were assembled as an initial monolithic feed rod for extrusion. The piston extruder was used for continual extrusion of tubes at 120 °C through a nozzle, with outer and inner diameters of 10 and 8 mm, respectively. The extrusion rate and pressure were 2–3 mm/s and 70 MPa, respectively. The tubes were cut into pieces of 1 m in length.

2.3. Thermal treatment of LWO and LWOMo extruded tubes and membranes

Thermoplastic binder removal was performed in a vertical tubular furnace with a heating rate fixed at 0.5 °C/min up to 200 °C, 0.1 °C/min up to 550 °C and 0.5 °C/min up to presintering temperature between 1100 and 1200 °C for 2 h.

Some of the debinded tubes were functionalized with thin film of lanthanum tungstate membrane layers with intermediate presintering step at 1000 °C (Section 2.4).

Final sintering step of sole support tubes and lanthanum tungstate based membranes was established through optimizing maximum temperatures within the range from 1400 °C to 1500 °C and dwell times within 3–10 h. Heating/cooling rates during sintering step were fixed to 1 °C/min.

Compressed air gas (1 L/min) was used to flush the furnace during all the thermal treatment (debindering, presintering and sintering) cycles.

Manufacturing of relatively long tubes/membranes (up to 500 mm in length) involves addressing the specific challenges related high temperature heat treatments. In this case, to prevent defect formation due to a non-homogeneous temperature gradient or due to non-uniform placement in the furnace during high-temperature treatments, the tubes were sintered vertically within a homemade alumina container which was protecting tubes from nonuniform temperature distribution.

2.4. Deposition of thin film lanthanum tungstate membrane

The deposition of thin film dense LWO56 composition membrane layer was performed on tubular supports with LWO56, LWO54 or

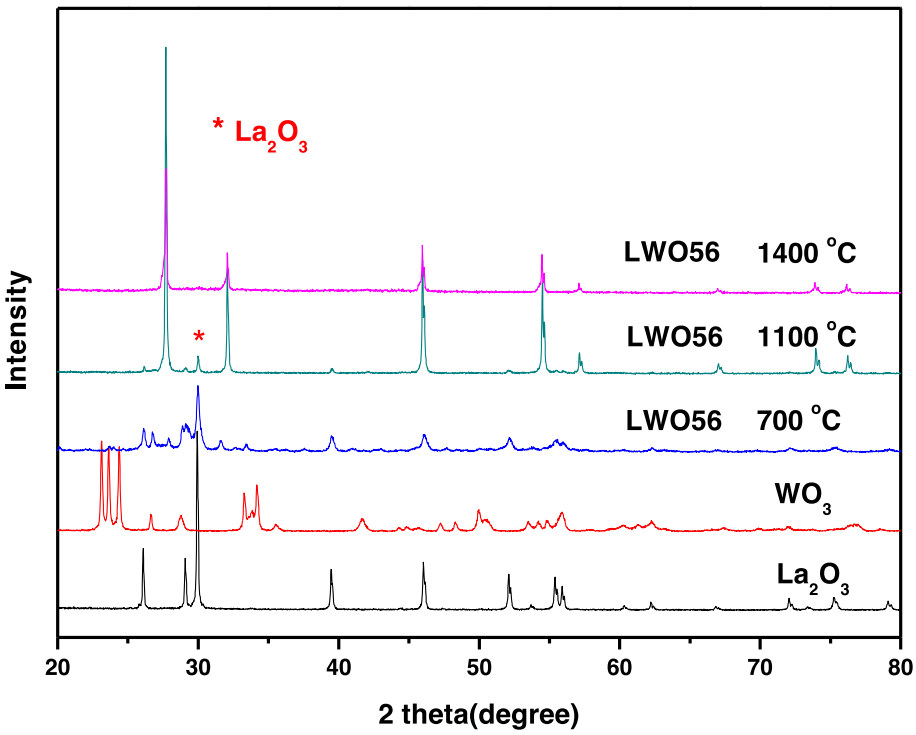

Fig. 1. XRD patterns of the LWO56 composition solid state reaction powder treated at different temperatures.

LWOMo compositions which were previously presintered. Full details related to colloidal suspension optimization and deposition procedure of thin film lanthanum tungstate membrane are given elsewhere [17].

2.5. Characterization

The phase composition of the as-synthesized un-substituted/Mo-substituted lanthanum tungstate powders and as-sintered materials was studied by X-ray powder diffraction (XRD) using Cu $K\alpha_1$ radiation (1.54056 Å, Bruker AXS D8 FOCUS diffractometer with a LynxEye PSD). The scans were collected at room temperature in the 2θ range (20–80°) with 0.02° step. The morphologies of the as-synthesized powders and the average particle size were estimated using scanning electron microscopy (LV-SEM, S–3400 N; Hitachi, Tokyo, Japan). Thermogravimetrical analysis (STA 449C; Netzsch, Selb, Germany) of the extruded green tube was performed in air up to 1000 °C at a heating rate of 2 °C/min. Microstructural studies of surfaces and fractural cross sections of debinded and sintered porous tubes and full membranes were done by scanning electron microscopy (LV-SEM, S–3400 N; Hitachi, Tokyo, Japan). ImageJ software was used to quantify the porosity and estimate the pore size distribution of the sintered tubes by image analysis.

The possible tungsten evaporation during sintering of the un-substituted and Mo-substituted lanthanum tungsten porous support tubes and full membranes was studied using electron probe Micro Analyzer (JXA-8500F; JEOL, Tokyo, Japan). Microanalyses were carried out on polished cross-sections of LWOMo and LWO56 samples sintered at 1500 °C for 2 h. The gas permeability measurements were carried out to quantify the gas permeability of the sintered porous support tubes according to Darcy equation, using an in-house built system [20]. The setup consists of a gas supply unit, a testing chamber and a unit for measuring the flow of the gas that permeates the sample to be measured. The sintered porous support tubes were mounted using soft rubber rings within a tubular chamber leaving one side exposed to air at ambient pressure and another side exposed to pressurized synthetic air. The measurements were made with a pressure difference ranging from 0.5 to 2 bar at room temperature and with synthetic air as the permeate gas. The uncertainty of the recorded steady state gas flux (J) and pressure at the pressurized part of the chamber was of 0.001 kg m^{-2} s^{-1} and 0.1 bar, respectively.

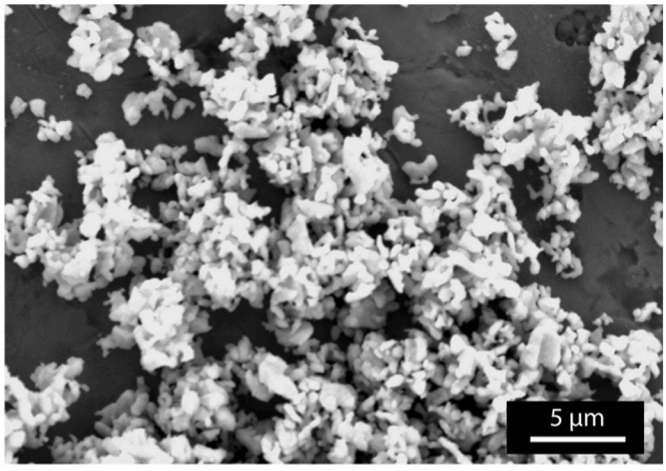

Fig. 2. SEM micrograph of the LWO56 as-synthesized powders calcined at 1100 °C and ball milled for for 24 h in ethanol media.

3. Results and discussion

3.1. Characterization of as-synthesized LWO and LWOMo powders

A conventional solid state reaction route to un-substituted and Mo-substituted lanthanum tungsten oxide powders was developed. This is the most widely used economic method in many industrial applications for the synthesis of polycrystalline powders from a mixture of solid starting materials.

The first indication of the early crystallization of the cubic phase from the amorphous matrix is observed at 700 °C as shown in Fig. 1 for LWO56 composition, although part of this inorganic matrix might

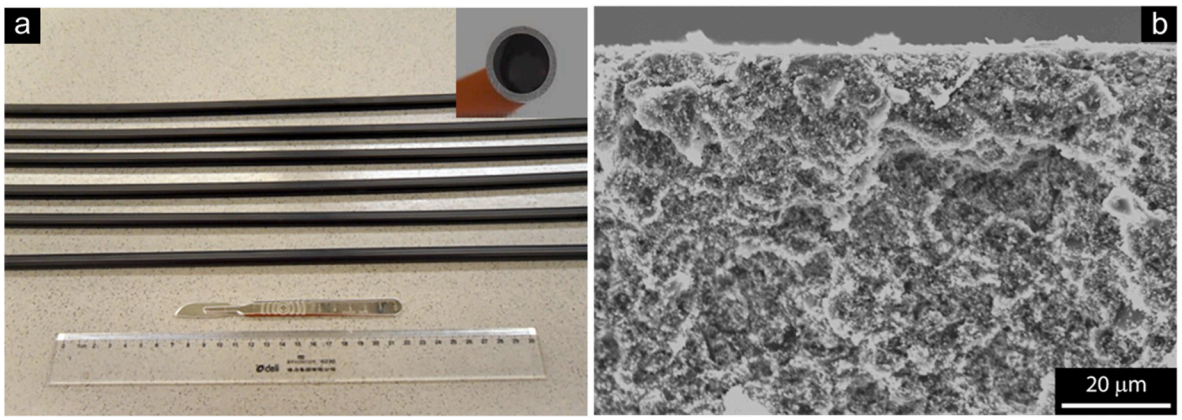

Fig. 3. Green state tubes obtained from LWOMo composition thermoplastic paste: a) Photographs of the as-prepared tubes (inclusion shows fractured cross section of the tube) and b) SEM micrograph of fracture cross section area close to the outer area. (For interpretation of the references to colour in this figure legend, the reader is referred to the Web version of this article.)

remain amorphous (La_2O_3). The patterns after calcination at low temperature show a considerable peak broadening (low crystallinity). This observation is in accordance with the results reported by Magrasó et al. [33] and supports that lanthanum tungstate is entropy stabilized as claimed by Yoshimura et al. [34]. The X-ray diffraction analysis of LWO54, LWOMo powders after calcining at 1100 °C for 2 h and sintering at 1400 °C for 5 h showed identical patterns to the LWO56 composition (please see supplementary material). A minor amount of unreacted La_2O_3 is still present at all compositions studied after calcination at 1100 °C, however it reacts completely to form a single cubic phase at 1400 °C as confirmed by the X-ray diffraction pattern.

Fig. 2 shows the typical morphology of the as-synthesized powders calcined at 1100 °C after ball-milling step. For all the compositions studied, the as-synthesized and ball milled powders presented very fine and well-structured particles, with characteristic sphere-type shape and particle sizes ranging within relatively narrow ~1 μm range. It is to note that lower La/W ratio or molybdenum substitution did not affect the morphology and particle size distribution of the as-synthesized powders.

Achieved chemical composition and uniform particle size distribution of raw materials indicate the ability of the established solid state reaction method and posterior powder conditioning to produce high quality desired composition raw powders. Following this, unsubstituted and Mo-substituted lanthanum tungstate powders were deployed for posterior processing of high temperature proton conducting membrane reactors.

3.2. Thermoplastic extrusion of green state tubes

After initial trials of inorganic phase homogenization, the procedure based on ball milling of obtained lanthanum tungstate powders with carbon black powders (sacrificial pore formers) for 24 h in ethanol media and drying prior mixing with thermoplastic carriers was established. The mixing and kneading process deployed was based on the use of an extrusion die with multiple narrow opening which produced continuous "spaghetti" shape rods with approximate diameter of 2 mm. This kneading process was repeated 4 times, the minimum which was needed to achieve highly homogeneous thermoplastic feed.

Inorganic phase homogenization step and their mixing with

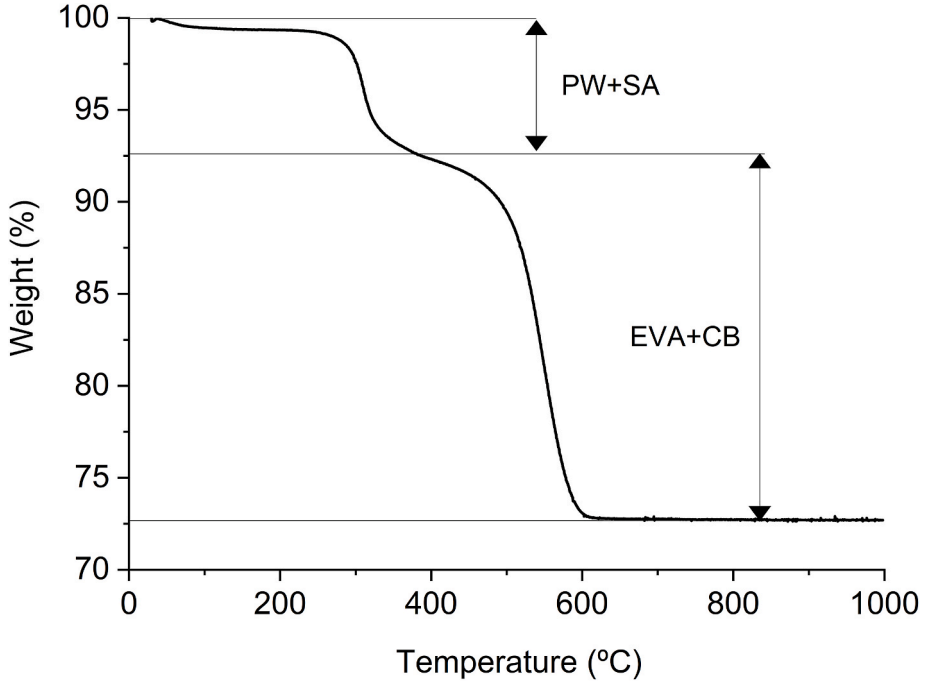

Fig. 4. Thermogravimetric curve of lanthanum tungstate based paste with paraffin wax (PW), stearic acid (SA), ethylene-vinylacetate (EVA) and carbon black (CB).

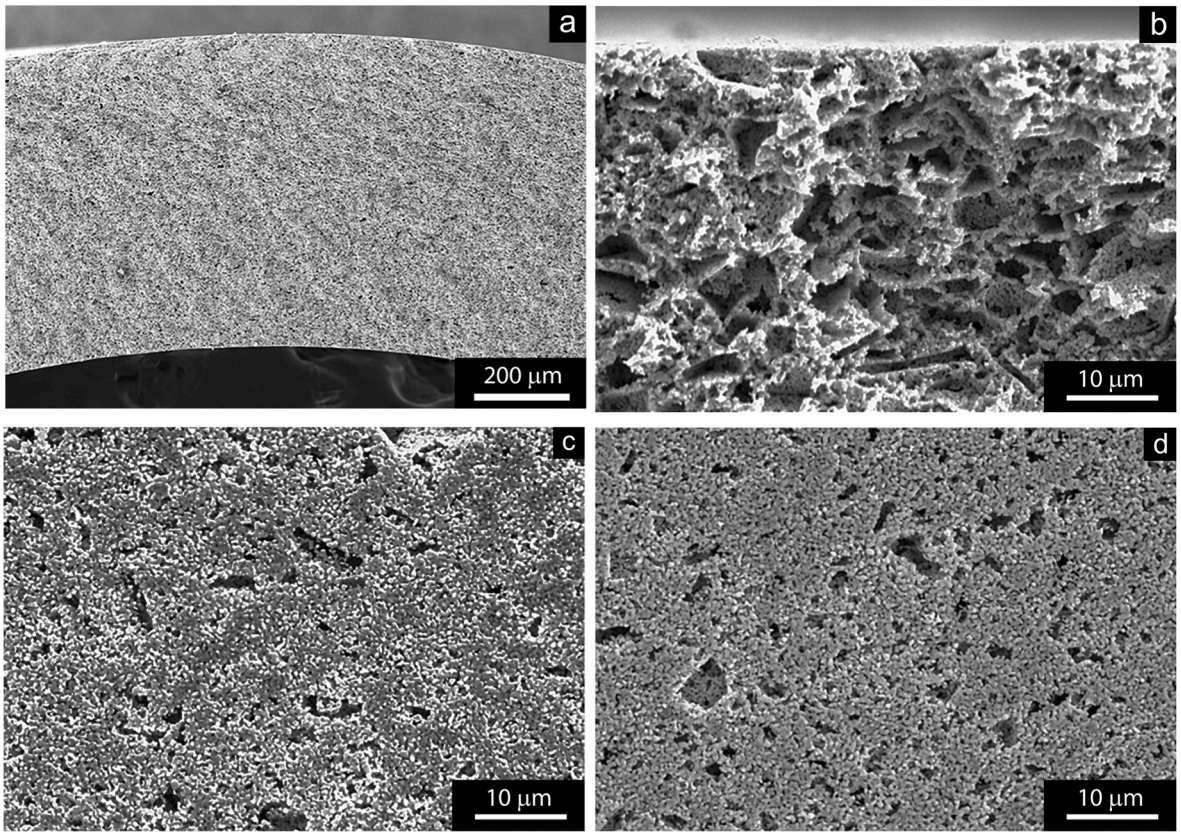

Fig. 5. SEM micrographs of LWOMo tube after calcination and presintering step at 1150 °C: (a, b) cross-section, (c) inner and (d) outer surface.

thermoplastic carriers through deployed kneading process showed to improve the behaviour of thermoplastic compounds under extrusion and most importantly, enhanced the uniform distribution of inorganic phases and resulted in low tortuosity/very smoot surface finish of porous support tubes. This was highly beneficial because allowed to perform the deposition of thin film dense functional layer directly on presintered porous supports, without the need of intermediate surface smoothening layers.

From the perspective of defined geometry control, the thermoplastic extrusion of tubes in vertical direction and their subsequent cooling just below the nozzle enabled the preparation of non-deformed tubes. The tube ovality and axial deflection depended in the first place on correct nozzle alignment, i.e., on the uniform wall thickness of the tube. Non-uniform wall thickness led to the extruded tube being bent in the direction of the thinner wall, either immediately after extrusion or later during sintering. It is to note that the disadvantage of thermoplastic extrusion in the vertical direction was that the tube became narrower with increasing length of the extruded tube. That is, the weight of the extruded tube loaded the plastic area of the tube just below the nozzle and reduced the tube diameter and wall thickness. The best results were obtained on extruding the mixture with the lowest nozzle temperature (120 °C) and low extruder revolutions (30 min^{-1}).

The appearance of the typical LWOMo extruded long tubes is shown in Fig. 3a, where the long straight tubes are shown. The outer diameter of the green state tubes was 10 mm and the inner diameter was 8 mm (the wall thickness was 1 mm). A SEM micrograph of fractured cross-section of the as extruded green state tube is show in Fig. 3b. The homogenous microstructure with a uniform distribution of solid phases and thermoplastic carriers is achieved.

The limit for reducing the extruder temperature during extrusion was the maximum admissible extruder power input to move the extruder piston, which increased with decreasing temperature due to higher viscosity of thermoplastic paste. It is to note that during homogenization step, higher temperatures and, above all, faster extruder piston speed improved the mixing process. Nevertheless, during the extrusion step higher temperatures and faster speeds resulted in rough surface finish, a highly detrimental feature in addition to problematic geometry control as described previously.

3.3. Design of debindering and pre-sintering process

In this work, a thermal debindering and pre-sintering in air at atmospheric pressure was carried out, to remove thermoplastic binders (PW, SA and EVA) and pore former (CB). Thermoplastic binder burnout is one of the most critical steps in thermoplastic extrusion process since removing the organic binders from the extruded tubes often gives rise to defects, especially when fine ceramic powder is used in combination of sacrificial pore formers.

The most suitable heating cycle was designed by means of thermogravimetrical analysis of the thermoplastic feedstock. As shown in Fig. 4, the decomposition of the binder occurs in two steps. The first weight loss stage, about 25 wt% of the total loss in the temperature range of 200–350 °C is attributed to the degradation of paraffin wax

and stearic acid in the binder system. The second stage between 350 and 550 °C is associated to the degradation of EVA and CB. The total weight loss percent (~28 wt%) corresponds to total organic component of the thermoplastic feedstock (~30 wt%). According to these results the debindering heating program was designed as follows: below 200 °C, a relatively quick heating rate of 0.5 °C/min was chosen taking into account that higher heating rates will cause cracking in the samples and lower heating rates will unnecessarily increase the debindering time. A slower heating rate of 0.1 °C/min was determined as the optimum rate between 200 and 550 °C to prevent surface cracks and internal bubbles through final debinding step. Finally, the tubes were heated at a heating rate of 0.5 °C/min to temperatures of 1100–1200 °C (dwell 2 h) to perform presintering step and achieve structural robustness and ease of

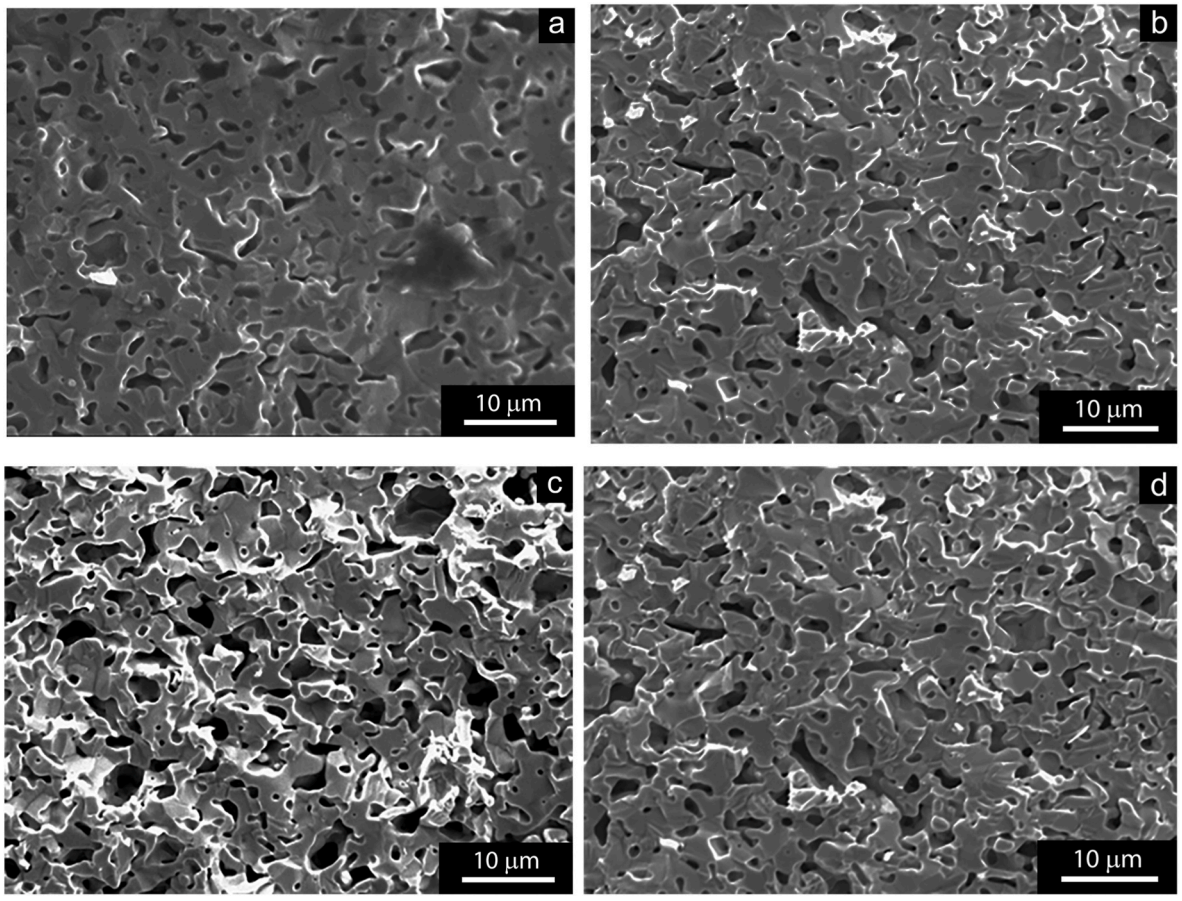

Fig. 6. SEM micrographs of fracture cross sections corresponding to the microstructures of LWOMo tubes sintered at (a) 1500 °C- 3 h, (b) 1490 °C- 3 h, (c) 1480 °C- 3 h and (d) 1470 °C - 3 h.

manipulation of the tubes during functional layer deposition to form final membrane structure.

All lanthanum tungstate based compositions showed identical behaviour under debinding and presintering steps, and as example case microstructures of LWOMo tubes are shown in Fig. 5. Interestingly, there is almost no shrinkage after presintering cycle employed (up to 1200 °C) as the tubular wall thickness is about 1 mm (Fig. 5a). The cross section micrograph showed the formation of uniform porous microstructure obtained after pre-sintering (Fig. 5b). The inner and outer surface morphologies were smooth and no cracks were present (Fig. 5c and d,

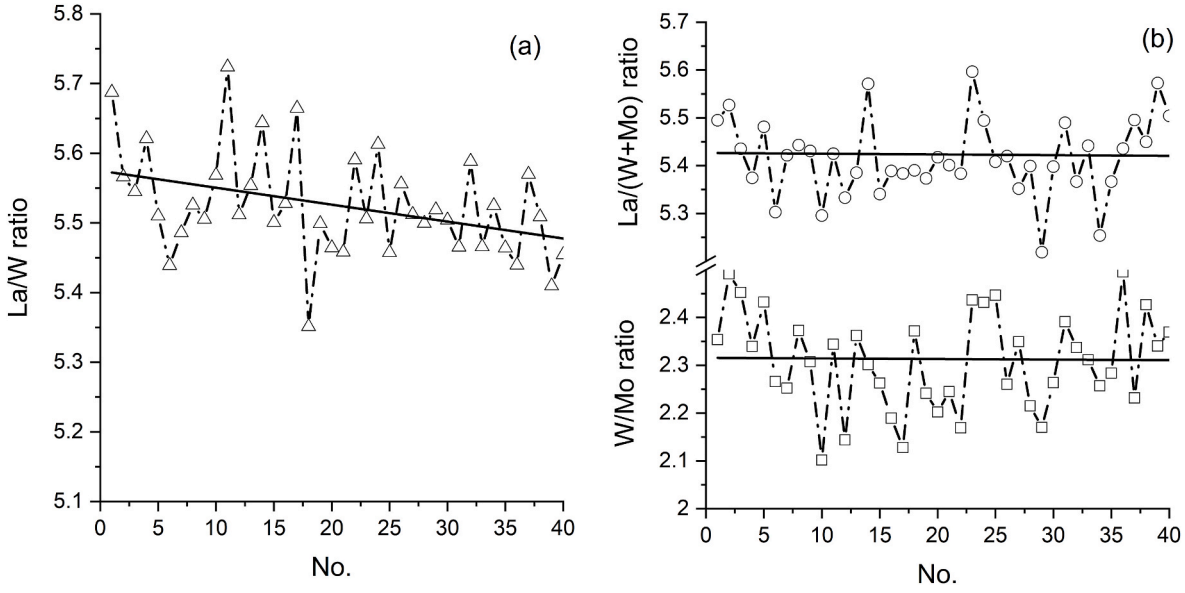

Fig. 7. Microanalysis results lanthanum tungstate composition pellets after thermal treatment at 1500 °C - 2 h. Data corresponding to a) samples with La/W ratio of 5.6 and b) samples with Mo-substitution.

Table 1
Average grain size, mean pore size and total porosity volume for the lanthanum tungstate based tubes sintered at 1450 °C - 10 h.

	Average grain size (μm)	Mean pore size (μm)	Total porosity (vol%)
LWO56	4.1 ± 0.3	10.1	24
LWO54	4.4 ± 0.3	7.3	23
LWOMo	5.1 ± 0.2	3.9	23

respectively).

Nevertheless, the formation of longitudinal cracks on the extremes of the long tubes with the signs of the spalling was observed, the signs of inefficient evacuation of gaseous phases which was limited to these areas of the tubes. Knowing that the heating profiles have a strong influence on the formation of these type of defects, the cause of these defects was attributed to nonhomogeneous temperature distribution. To prevent the formation of these defects during high-temperature processes owing to a nonhomogeneous temperature field in the furnace, the tubes were placed in alumina housing which had openings to facilitate the evacuation of gaseous phases formed from organic binders and pore former burnout. The shielding effect produced by the alumina housing was sufficient to homogenize temperature distribution during applied thermal treatments and it also avoided possible contamination of the tubes from furnace lining.

After applying the optimized debindering and pre-sintering cycles on long tubes (~500 mm) a defect free tubular supports were achieved, indicating the effectiveness of developed debindering and pre-sintering route to obtain lanthanum tungstate based supports in an acceptable period of time.

3.4. Effect of the sintering temperature

Presintered lanthanum tungstate-based tubular supports were subjected to the final thermal treatment process at temperatures ranging from 1400 °C to 1500 °C and varying dwell times at maximum temperature. To evaluate the effects of the sintering cycle trials on microstructural porosity and compositional changes due to possible tungsten evaporation at high temperature, pellet and short (~20 mm) tubular samples were used.

The effect of the sintering temperature on the microstructure can be observed in Fig. 6. As a similar trend was observed for all the compositions, only those micrographs corresponding to LWOMo composition samples are shown. As expected, the total porosity decreases from 28 to 21 vol% when the sintering temperature is increased from 1470 to 1500 °C (dwell times of 3 h). It is to note that sintering temperature variation even in relatively narrow gap of 30 °C, led to a considerable variation in average grain sizes. That is, the average grain size increased from 5 μm to almost 10 μm when sintering temperature was increased from 1470 °C to 1480 °C. Whereas, further increase in a sintering temperature up to 1500 °C led to a further grain size growth, reaching values of 30–50 μm.

Apart from considerable microstructural changes, tungsten evaporation due to applied high temperature thermal treatments could lead to undesirable compositional changes. To address this issue, pellet type samples from thermoplastic feedstocks with varying lanthanum tungstate composition were prepared and their chemical composition was characterized after exposure to high temperature thermal treatments. Microanalysis results on LWO56 sintered pellets confirm that the La/W ratio = 5.57 was close to nominal ratio (La/W = 5.6) even after exposures to temperatures as high as 1500 °C and dwell time of 2 h (Fig. 7a). Similarly, in case of samples with Mo-substitution, there were no signs of tungsten evaporation and La/(W + Mo) = 5.41 with W/Mo = 2.31 were achieved, which was very close to nominal ratio for LWOMo composition (5.4 and 2.33 respectively) as shown in Fig. 7b.

Even though no evaporation of tungsten phase was detected, further work on sintering cycle optimization of lanthanum tungstate based porous supports was limited to maximum temperature of 1450 °C with varying dwell times. This was done to limit the microstructural changes in the form of grain growth and to preserve the overall porosity of the porous supports. Table 1 reports the average grain size, mean pore size and total porosity estimated by image analysis from polished cross sections of lanthanum tungstate-based tubes sintered at 1450 °C with the dwell time of 10 h The average grain size increases with molybdenum substitution and tungsten content, whereas the mean pore size

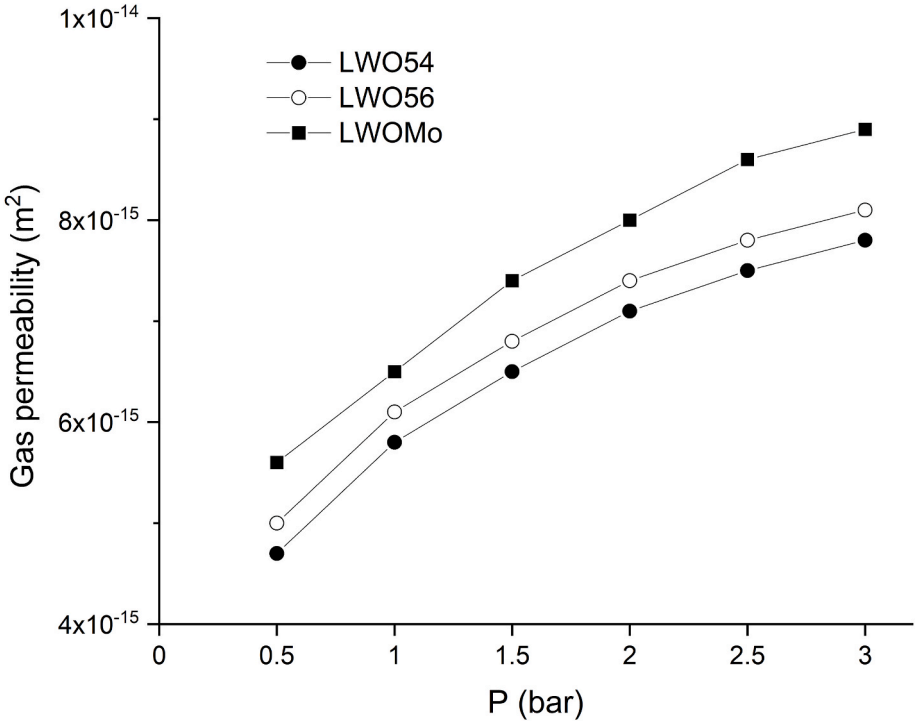

Fig. 8. The measured gas permeability for the lanthanum tungstate based tubes sintered at 1450 °C - 10 h.

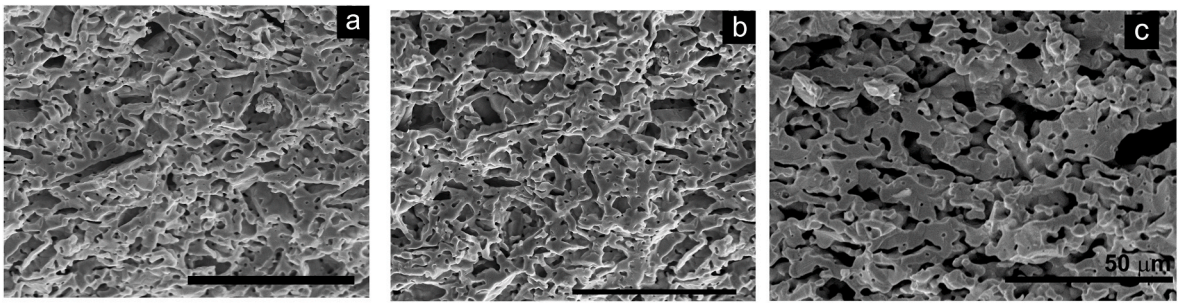

Fig. 9. SEM micrographs of fracture cross sections of lanthanum tungstate-based tubes at 1450 °C - 10 h: (a) LWO56, (b) LWO54 and (c) LWOMo.

decreases. The LA/W or W/Mo ratio do not affect the total porosity amount.

The measured gas permeabilities for these lanthanum tungstate tubes are presented Fig. 8. The permeability decreases when decreasing La/W ratio and increasing Mo-substitution. The reason for the higher permeability for LWO56 is due to the increase in open porosity, bigger mean pore sizes and better pore connectivity which may enhance the gas transport pathway, in agreement with the results presented in the Table 1.

SEM micrographs of fracture cross sections corresponding to LWO56, LWO54 and LWOMo composition tubular samples sintered at 1450 °C with 10 h of dwell time are shown in Fig. 9. Defect free and homogeneous lanthanum tungstate-based structures with relatively uniform microstructural features were obtained (please see supplementary material). In agreement with the XRD results, free of impurities or phase segregations at the grain boundaries compositions were achieved.

It is to note, that even though the porosity was reduced to the range of 23–24 vol%, highly permeable microstructures with low necking were formed, suitable for deployment as structural supports of high temperature temperature H_2 separation applications. The gas permeability of the produced tubular supports was in the range of 6×10^{-15} m^2 at 1 bar overpressure, which is aligned (or even higher) than those reported for supports of high flux oxygen transport membranes [27]. The permeability of the asymmetric membranes was similar to previous measurements of planar membranes with LWO56 composition [16].

To evaluate the effects of the sintering cycle on macrostructural features of tubular supports, that is the deformations and irregularities in geometry, longer samples with minimum length of 100 mm were used. The subject of investigation was the largest and smallest wall thickness, the tube sagging (i.e. deflection from the straight line at the tube centre), the tube narrowing (i.e. the difference between the diameters at the beginning and end of the tube) and the tube ovality (i.e. the difference between the largest and the smallest diameter of the tube).

After sintering cycle (1450 °C with 10 h), the outer diameter of sintered tubes was reduced to 7.4–7.6 mm and obtained average wall thickness was in the range of 0.75–0.8 mm. The observed variation was mainly due to compositional changes resulting in the highest contraction for the LWOMo composition tubes. It is to note that in the case of ~100 mm length samples it was possible to obtain tubes with uniform wall thickness for all compositions and the difference in the wall thickness of sintered tubes of the same composition did not exceed 50 µm. The irregular ovality along the as extruded tube length was responsible for the maximum deflection of 1 mm measured for these tubes.

In case of longer tubes (>100 mm), signs of high temperature creep could be observed due to a denser microstructure formation at the bottom of the tube. Therefore, the further work on H_2 separation membranes was limited to samples with 100 mm in length.

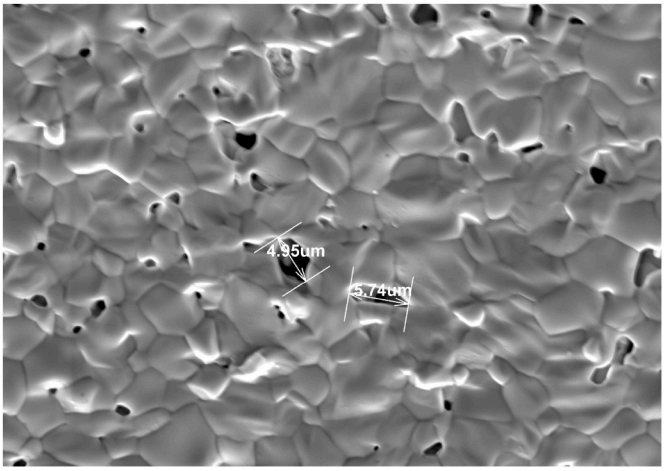

Fig. 10. SEM micrograph of the pinhole type defects formed within LWO56 functional layer which was co-sintered directly on green state tubular support. Defect formation is attributed to evacuation of gases during debindering and calcination step.

3.5. Dip-coating of the supports and co-sintering of the asymmetric H_2 separation membranes

Co-sintering process is the preferred method for fabrication of multilayer solid oxide structures including tubular membranes. The reduction of the number of thermal treatment steps, which impacts directly into the time and manufacturing cost of the membranes, is seen as the most important criteria to consider co-sintering as suitable for mass-scale production. Therefore, once the optimal conditions for the sintered supports are defined, the deposition of a dense thin and defect free layer should be addressed. The deposition procedure and consecutive thermal treatment steps should be optimized having in mind that the preservation of the porous microstructure of the support is a must for optimal performance of asymmetric membranes.

In this work, co-sintering process was optimized to fabricate LWO56 composition dense membranes onto LWO and LWOMo tubular supports. The deposition of functional layer was done through dip coating of stable LWO56 composition powder colloidal suspension, aiming to form asymmetric membranes with fully dense ~ 20 µm thick outer layer while preserving porous support microstructure.

Attempts to co-sinter directly functional LWO56 layers deposited on green state LWO56, LWO54, LWOMo tubular supports resulted in leaky membranes exhibiting transversal pores as a consequence of the defects formed by the gases released during the debindering and calcination step (burnout of thermoplastic binders and pore formers) (Fig. 10). Same issue has been reported in other studies, where different composition green state supports were coated with functional layers to form dense asymmetric membranes [35–37].

As an alternative route, calcined LWO56, LWO54 and LWOMo

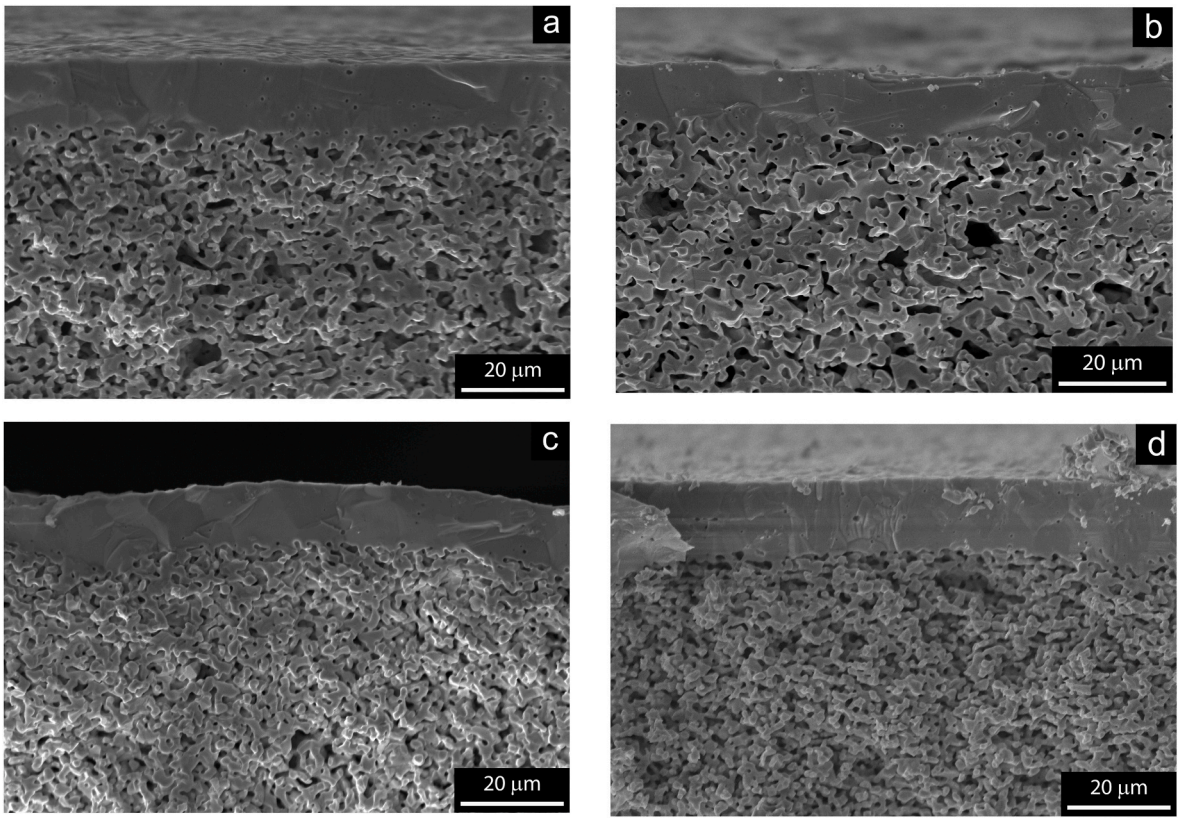

Fig. 11. SEM micrographs showing fracture cross section of LWO56 dense membranes on top of porous support tubes: a) membrane with LWO56 support co-sintered at 1450°C – 6h, b) membrane with LWO54 support co-sintered at 1450°C – 6h, c) membrane with LWOMo support co-sintered at 1450°C – 6h and d) membrane with LWOMo support co-sintered at 1425°C – 6h. The black areas are pores.

composition tubular supports (see section 3.3) were dip coated on an outer surface using LWO56-based colloidal suspension. The process was repeated one more time after presintering step which was performed at 1000 °C. Finally, sintering cycle was applied following findings from tubular porous support sintering cycle optimization.

After sintering cycles, an outer surface of the membranes showed defect free and shiny surface finish, indicating the formation of dense functional layer. The microstructural observation through SEM of prepared membranes confirmed the formation of a dense functional layer and preservation of permeable support microstructure. Fig. 11a shows the fracture surface of LWO56 composition membrane the same composition tubular support, where defect free and gas tight layer with approximate thickness of ~20 μm was formed after sintering step of 1450 °C – 6h. Almost identical asymmetric membrane microstructural features were obtained for LWO56 composition membrane sintered on LWO54 composition tubular support (Fig. 11b). Whereas, in the case of membranes with LWOMo support, the higher densification of porous support is observed when sintering cycle with maximum temperature 1450 °C – 6h is used (Fig. 11c). In this case, the reduction of sintering temperature to 1425 °C – 6h was sufficient to achieve dense and defect free LWO56 composition functional layer while preserving highly porous LWOMo support microstructure (Fig. 11d).

The previously observed tendency for a grain growth and creep at elevated temperatures of lanthanum tungstate-based materials had a favorable role in this case to consolidate the dense microstructure from nearby packed particles. Meanwhile, in the case of porous supports, the deployment of sacrificial pore former and thermoplastic feedstock resulted in highly porous starting microstructures which were successfully preserved after sintering step.

The interface between the LWO56 membrane layer and porous supports, a critical feature which dramatically reduces contact loss, consisted of a superior adhesion for all asymmetric membranes.

How this microstructure impacts on the performance of the membranes will be discussed in a later publication, however, we can anticipate that the performance of LWO56 tubular asymmetric membranes is comparable to the previous work published in planar geometry asymmetric membranes [16].

4. Conclusions

In order to establish the manufacturing route for high temperature proton conducting ceramics to be used in catalytic membrane reactors for synthetic fuel from gas-to-liquid (GTL) processes, a high-quality lanthanum tungstate (LWO)-based support tubes were fabricated by a cost-effective solid-state synthesis and thermoplastic extrusion processes. Obtained long, porous substrates presented microstructures with high pore-connectivity and small grain sizes (~ 4 μm), resulting in gas permeation values as high as 6.5 x 10^{-15} m^2 at 1 bar overpressure. Optimized deposition conditions of dense functional layers led to formation of defect free and gas tight layers with approximate thickness of 20 μm.

According to the results of this work, the grain boundary mobility for lanthanum tungstate (LWO)-based compositions increases with increasing tungsten content and Mo substitution, whereas the mean pore size decreases.

Declaration of competing interest

The authors declare that they have no known competing financial interests or personal relationships that could have appeared to influence the work reported in this paper.

Acknowledgments

Financial support from the Research Council of Norway (grant no. 195912/S10) is gratefully acknowledged.

Appendix A. Supplementary data

Supplementary data to this article can be found online at https://doi.org/10.1016/j.oceram.2022.100226.

References

[1] S.H. Morejudo, R. Zanón, S. Escolástico, I. Yuste-Tirados, H. Malerød-Fjeld, P. K. Vestre, W.G. Coors, A. Martínez, T. Norby, J.M. Serra, C. Kjølseth, Direct conversion of methane to aromatics in a catalytic co-ionic membrane reactor, Science 80– (2016) 353, https://doi.org/10.1126/science.aag0274.

[2] J.W. Phair, S.P.S. Badwal, Review of proton conductors for hydrogen separation, Ionics (Kiel) 12 (2006) 103–115, https://doi.org/10.1007/s11581-006-0016-4.

[3] H. Iwahara, Y. Asakura, K. Katahira, M. Tanaka, Prospect of hydrogen technology using proton-conducting ceramics, Solid State Ionics 168 (2004) 299–310, https://doi.org/10.1016/j.ssi.2003.03.001.

[4] X. Dong, W. Jin, N. Xu, K. Li, Dense ceramic catalytic membranes and membrane reactors for energy and environmental applications, Chem. Commun. 47 (2011) 10886–10902, https://doi.org/10.1039/C1CC13001C.

[5] C. Athanassiou, G. Pekridis, N. Kaklidis, K. Kalimeri, S. Vartzoka, G. Marnellos, Hydrogen production in solid electrolyte membrane reactors (SEMRs), Int. J. Hydrogen Energy 32 (2007) 38–54, https://doi.org/10.1016/j.ijhydene.2006.06.031.

[6] C. Sg, G. Vk, L. Jys, Synthesis and hydrogen permeation properties of asymmetric proton-conducting ceramic membranes, Solid State Ionics 176 (2005) 2653–2662, https://doi.org/10.1016/j.ssi.2005.07.005.

[7] H. Yoon, T. Oh, J. Li, K.L. Duncan, E.D. Wachsman, Permeation through $SrCe_{0.9}Eu_{0.1}O_{3-\delta}$/Ni–$SrCeO_3$ tubular hydrogen separation membranes, J. Electrochem. Soc. 156 (2009) B791, https://doi.org/10.1149/1.3121209.

[8] H. Matsumoto, S. Okada, S. Hashimoto, K. Sasaki, R. Yamamoto, M. Enoki, T. Ishihara, Hydrogen separation from syngas using high-temperature proton conductors, Ionics (Kiel) 13 (2007) 93–99, https://doi.org/10.1007/s11581-007-0080-4.

[9] R. Haugsrud, T. Norby, Proton conduction in rare-earth ortho-niobates and ortho-tantalates, Nat. Mater. 5 (2006) 193–196, https://doi.org/10.1038/nmat1591.

[10] R. Haugsrud, T. Norby, High-temperature proton conductivity in acceptor-doped $LaNbO_4$, Solid State Ionics 177 (2006) 1129–1135, https://doi.org/10.1016/j.ssi.2006.05.011.

[11] R. Haugsrud, Defects and transport properties in Ln_6WO_{12} (Ln = La, Nd, Gd, Er), Solid State Ionics 178 (2007) 555–560, https://doi.org/10.1016/j.ssi.2007.01.004.

[12] M.E. Ivanova, W. Deibert, D. Marcano, S. Escolástico, G. Mauer, W.A. Meulenberg, M. Bram, J.M. Serra, R. Vaßen, O. Guillon, Lanthanum tungstate membranes for H_2 extraction and CO_2 utilization: fabrication strategies based on sequential tape casting and plasma-spray physical vapor deposition, Separ. Purif. Technol. 219 (2019) 100–112, https://doi.org/10.1016/j.seppur.2019.03.015.

[13] S. Escolastico, J. Seeger, S. Roitsch, M. Ivanova, W.A. Meulenberg, J.M. Serra, Enhanced H_2 separation through mixed proton-electron conducting membranes based on $La_{5.5}W_{0.8}M_{0.2}O_{11.25-\delta}$, ChemSusChem 6 (2013) 1523–1532, https://doi.org/10.1002/cssc.201300091.

[14] M. Amsif, A. Magrasó, D. Marrero-López, J.C. Ruiz-Morales, J. Canales-Vázquez, P. Núñez, Mo-substituted lanthanum tungstate $La_{28-y}W_{4+y}O_{54+\delta}$: a competitive mixed electron–proton conductor for gas separation membrane applications, Chem. Mater. 24 (2012) 3868–3877, https://doi.org/10.1021/cm301723a.

[15] S. Zhan, X. Zhu, B. Ji, W. Wang, X. Zhang, J. Wang, W. Yang, L. Lin, Preparation and hydrogen permeation of $SrCe_{0.95}Y_{0.05}O_{3-\delta}$ asymmetrical membranes, J. Membr. Sci. 340 (2009) 241–248, https://doi.org/10.1016/j.memsci.2009.05.037.

[16] V. Gil, J. Gurauskis, C. Kjølseth, K. Wiik, M.A. Einarsrud, Hydrogen permeation in asymmetric $La_{28-x}W_{4+x}O_{54+3x/2}$ membranes, Int. J. Hydrogen Energy 38 (2013) 3087–3091, https://doi.org/10.1016/j.ijhydene.2012.12.105.

[17] V. Gil, J. Gurauskis, M.-A. Einarsrud, Asymmetric supported dense lanthanum tungstate membranes, J. Eur. Ceram. Soc. 34 (2014) 3783–3790, https://doi.org/10.1016/j.jeurceramsoc.2014.06.019.

[18] D. Montaleone, E. Mercadelli, S. Escolástico, A. Gondolini, J.M. Serra, A. Sanson, All-ceramic asymmetric membranes with superior hydrogen permeation, J. Mater. Chem. A. 6 (2018) 15718–15727, https://doi.org/10.1039/C8TA04764B.

[19] S. Hamakawa, Synthesis and hydrogen permeation properties of membranes based on dense $SrCe_{0.95}Yb_{0.05}O_{3-\alpha}$ thin films, Solid State Ionics 148 (2002) 71–81, https://doi.org/10.1016/S0167-2738(02)00047-4.

[20] M. Weirich, J. Gurauskis, V. Gil, K. Wiik, M.-A. Einarsrud, Preparation of lanthanum tungstate membranes by tape casting technique, Int. J. Hydrogen Energy 37 (2012) 8056–8061, https://doi.org/10.1016/j.ijhydene.2011.09.083.

[21] W. Deibert, M.E. Ivanova, W.A. Meulenberg, R. Vaßen, O. Guillon, Preparation and sintering behaviour of $La_{5.4}WO_{12-}$ asymmetric membranes with optimised microstructure for hydrogen separation, J. Membr. Sci. 492 (2015) 439–451, https://doi.org/10.1016/j.memsci.2015.05.065.

[22] Z. Liu, G. Zhang, X. Dong, W. Jiang, W. Jin, N. Xu, Fabrication of asymmetric tubular mixed-conducting dense membranes by a combined spin-spraying and co-sintering process, J. Membr. Sci. (2012) 415–416, https://doi.org/10.1016/j.memsci.2012.05.011, 313–319.

[23] K. Kwok, H.L. Frandsen, M. Søgaard, P.V. Hendriksen, Stress analysis and fail-safe design of bilayered tubular supported ceramic membranes, J. Membr. Sci. 453 (2014) 253–262, https://doi.org/10.1016/j.memsci.2013.11.020.

[24] X. Dong, W. Jin, Mixed conducting ceramic membranes for high efficiency power generation with CO_2 capture, Curr. Opin. Chem. Eng. 1 (2012) 163–170, https://doi.org/10.1016/j.coche.2012.03.003.

[25] K. Kwok, L. Kiesel, H.L. Frandsen, M. Søgaard, P.V. Hendriksen, Strength characterization of tubular ceramic materials by flexure of semi-cylindrical specimens, J. Eur. Ceram. Soc. 34 (2014) 1423–1432, https://doi.org/10.1016/j.jeurceramsoc.2013.12.005.

[26] Z. Zhu, J. Xiao, W. He, T. Wang, Z. Wei, Y. Dong, A phase-inversion casting process for preparation of tubular porous alumina ceramic membranes, J. Eur. Ceram. Soc. 35 (2015) 3187–3194, https://doi.org/10.1016/j.jeurceramsoc.2015.04.026.

[27] D.K. Ramachandran, M. Søgaard, F. Clemens, B.R. Sudireddy, A. Kaiser, Low cost porous MgO substrates for oxygen transport membranes, Mater. Lett. 169 (2016) 254–256, https://doi.org/10.1016/j.matlet.2016.01.142.

[28] M.L. Fontaine, C. Denonville, Z. Li, W. Xing, J.M. Polfus, J. Kvello, J.S. Graff, P. I. Dahl, P.P. Henriksen, R. Bredesen, Fabrication and H_2 flux measurement of asymmetric $La_{27}W_{3.5}Mo_{1.5}O_{55.5-\delta}$ – $La_{0.87}Sr_{0.13}CrO_{3-\delta}$ membranes, J. Eur. Ceram. Soc. 38 (2018) 1695–1701, https://doi.org/10.1016/j.jeurceramsoc.2017.11.015.

[29] M. Trunec, Fabrication of zirconia- and ceria-based thin-wall tubes by thermoplastic extrusion, J. Eur. Ceram. Soc. 24 (2004) 645–651, https://doi.org/10.1016/S0955-2219(03)00258-9.

[30] M.R. Ismael, F. Clemens, T. Graule, M.J. Hoffmann, Effects of different thermoplastic binders on the processability of feedstocks for ceramic co-extrusion process, Ceram. Int. 37 (2011) 3173–3182, https://doi.org/10.1016/j.ceramint.2011.05.084.

[31] G. Scheying, I. Wührl, U. Eisele, R. Riedel, Monoclinic zirconia bodies by thermoplastic ceramic extrusion, J. Am. Ceram. Soc. 87 (2004) 358–364, https://doi.org/10.1111/j.1551-2916.2004.00358.x.

[32] F. Clemens, T. Graule, Thin wall ceramic tubes by extrusion of thermoplastic-ZrO_2 compounds, Key Eng. Mater 206–213 (2002) 425–428. https://doi.org/10.4028/www.scientific.net/KEM.206-213.425.

[33] A. Magrasó, R. Haugsrud, Effects of the La/W ratio and doping on the structure, defect structure, stability and functional properties of proton-conducting lanthanum tungstate La28−xW4+xO54+δ. A review, J. Mater. Chem. A. 2 (2014) 12630–12641, https://doi.org/10.1039/C4TA00546E.

[34] M. Yoshimura, A. Rouanet, High temperature phase relation in the system La2O3WO3, Mater. Res. Bull. 11 (1976) 151–158, https://doi.org/10.1016/0025-5408(76)90070-2.

[35] D.K. Ramachandran, M. Søgaard, F. Clemens, J. Gurauskis, A. Kaiser, Fabrication and performance of a tubular ceria based oxygen transport membrane on a low cost MgO support, Separ. Purif. Technol. 147 (2015), https://doi.org/10.1016/j.seppur.2015.02.037.

[36] X. Yin, L. Hong, Z.-L. Liu, Asymmetric tubular oxygen-permeable ceramic membrane reactor for partial oxidation of methane, J. Phys. Chem. C 111 (2007) 9194–9202, https://doi.org/10.1021/jp0682917.

[37] T. Li, Z. Wu, K. Li, High-efficiency, nickel-ceramic composite anode current collector for micro-tubular solid oxide fuel cells, J. Power Sources 280 (2015) 446–452, https://doi.org/10.1016/j.jpowsour.2015.01.130.